Available online at www.sciencedirect.com

ScienceDirect

Current Opinion in
Colloid & Interface Science

Open issues in the linear and NonLinear rheology of wormlike micelles

Rossana Pasquino[a] and Rolando Castillo[b]

We review experimental evidence and theoretical/modeling approaches on Wormlike Micelles (WLMs) dynamics in linear and nonlinear regimes. We focus on recent works regarding the extraction of quantitative microscopic information from linear rheology data and the possibility of quantifying the fast relaxation processes. Models for WLMs undergoing reptation and chain sequence rearrangement are discussed. Strong shear and elongational flows that can cause interesting phenomena, *e.g.* chain scission, structure formation, and elastic instabilities in WLMs, are considered. More specifically, start-up shear flow in the nonlinear regime, LAOS experiments, and relative data treatment are discussed, together with shear-banding phenomena and their dynamics, inertio-elastic instabilities, and secondary flow. Different techniques for measuring WLMs in extensional flow are compared, referring in particular to the recent dripping-onto-substrate (DoS) extensional rheometry, which is able to address some shortcomings of the CaBER technique. We finally deal with the potential source of triggering flow profiles and secondary flows with fluid properties and external conditions.

Addresses
[a] Dipartimento di Ingegneria Chimica, dei Materiali e della Produzione Industriale - DICMaPI, Università degli Studi di Napoli Federico II, P.le Tecchio 80, 80125 Naples, Italy
[b] Instituto de Física, Universidad Nacional Autónoma de México, P.O. Box 20-364, 01000, Mexico City, Mexico

Corresponding authors: Pasquino, Rossana Pasquino (r.pasquino@unina.it); Castillo, Rolando (rolandoc@fisica.unam.mx)

Current Opinion in Colloid & Interface Science 2025, **77**:101919

This review comes from a themed issue on **Rheology (2024)**

Edited by **Ruth Cardinaels** and **Yujun Feng**

For complete overview about the section, refer Rheology (2024)

https://doi.org/10.1016/j.cocis.2025.101919

Wormlike micelles are fascinating self-assembled structures originating from the spontaneous grouping of surfactant molecules in polar/apolar solutions, which possess peculiar rheological properties that make them attractive in a wide range of products. They are prone to be used in oil fields for hydraulic fracturing, as drag-reducing agents and thickeners for personal and home care products, smart materials for nanobiotechnology, and reservoirs for drugs and nanofillers [1,2]. The design (via spontaneous molecular self-assembly) of materials with final characteristics defined in advance has been recognized as overriding to tune their final uses.

The first part of this review will be devoted to the multiple ways to guide wormlike micelles self-assemblies in surfactant solutions and their linear rheological response. This will be linked to the underlying microstructure and worms' mesoscopic length scales. The final part deals with the response of wormlike micelles to strong flows and the resulting mechanisms induced by the flow, such as scission and elastic instabilities.

The last twenty years have seen great advances in techniques and methods for understanding and describing the properties of wormlike micelles, particularly in linear and nonlinear rheology. Therefore, we had to manage the scope of this review to be short and at the same time to present the main advances, although that surely involves our personal point of view. Hence, we probably left many subjects without a proper and deep description, and we apologize for those omissions. Also, other reviews include points not addressed here that would be important to the readers [3–5].

Wormlike micelles self-assemblies: zero shear viscosity and cryo-EM imaging

Amphiphilic molecules (ionic surfactants, lipids, diblock copolymers, etc.) contain two or more chemically distinct moieties, covalently merged to form a single molecule. The incompatibility between the different units and solvents leads to local segregation and the consequent self-assembly[6]. Aggregates' morphology units can be tuned from spheres, cylinders, giant cylindrical micelles or wormlike micelles, vesicles, and bilayers by varying the blocks' chemical nature, molecular weight, temperature, ionic strength, etc. [7,8] The preferred surface geometry of the aggregates produces the so-called spontaneous curvature, which optimizes the most energetically adequate packing of the assembled aggregates, but it does not account for the effects of entropy. The aggregates' final shape also considers the effects of entropy on the assemblies to stabilize some structures and defects.

Beneath the critical micelle concentration (CMC) [9–11], entropy privileges a uniform dissolution of the building blocks in a solvent; aggregation is irrelevant. Above CMC, energetic interaction dominates, and translational entropy plays a minor role. Consequently, the number of aggregates, usually sphere-shaped, increases. In cylindrical micelles, the curvatures are moderate, lower than in a spherical micelle but higher than in bilayers. In cylindrical micelles, energy is improved when the curvature is unvarying, forming extended linear structures, *i.e.* the WLMs. Nevertheless, entropy introduces randomness by making curved cylindrical micelles, which increases conformational entropy (i.e., like in polymers) and through topological defects in the form of end-caps and/or branch junction. These defects are introduced by forming regions with different local curvatures but incurring in different energetic drawbacks. The entropic gain related to end-caps is greater than that of branch junctions[12]. However, while topological defects introduce an entropy gain, the dominating defect is given by spontaneous curvature produced by the amphiphiles. If the energy required to create two end-caps from a long cylinder, *i.e.* the scission energy of a cylindrical micelle is big, cylindrical micelles may change into quite long and intertwined at a relatively low total amphiphile volume fraction[7,13]. Therefore, the end-caps increase entropy by increasing the amount of micelles in the liquid solution, and a drop in the scission energy shortens the wormlike micellar length. Branch junctions expand the configurations, permitting percolation to form extended micellar networks, leading to a multi-connected net of cylindrical micelles. An assessment of junctions and end-caps can be found elsewhere[12].

Multiple ways exist to formulate aqueous solutions containing WLMs. Ionic surfactants with aliphatic chains of *ca.* 16 carbons can spontaneously pack into cylindrical micelles. Another chance to induce WLMs is to work at low surfactant concentration (above the CMC) and tune temperature or pH by encouraging spherical micelles to self-assemble in a cylindrical shape[14–16]. Additives have also been widely explored in the last decades [17], particularly concerning binding (also called penetrating) additives. They are complex molecules characterized by at least one aromatic ring in their molecular structure and by the possible combined presence of a charge (binding salts or hydrotropes)[5,18]. Binding salts combine two actions, one related to the penetration of the molecule into the micellar structure self-assembly (inducing an effective change in the surfactant molecules' apparent size) and the other to the electrostatic screening activity among micelles[19]. Incorporating these cosolutes, by tuning their molecular structure and counterions allows to modulate intermolecular interactions, consequently inducing morphological transitions in a controlled way [18,20–22], as shown schematically in Figure 1.

Cryo-Transmission Electron Microscopy (Cryo-TEM) is the most accomplished technique able to differentiate between various architectures, such as linear and branched WLMs, with similar rheological responses [23–26]. Indeed, entangled linear and branched micelles cannot be distinguished in neutron or light scattering and flow-induced birefringence. Although cryo-TEM imaging is needed for a detailed microstructural

Figure 1

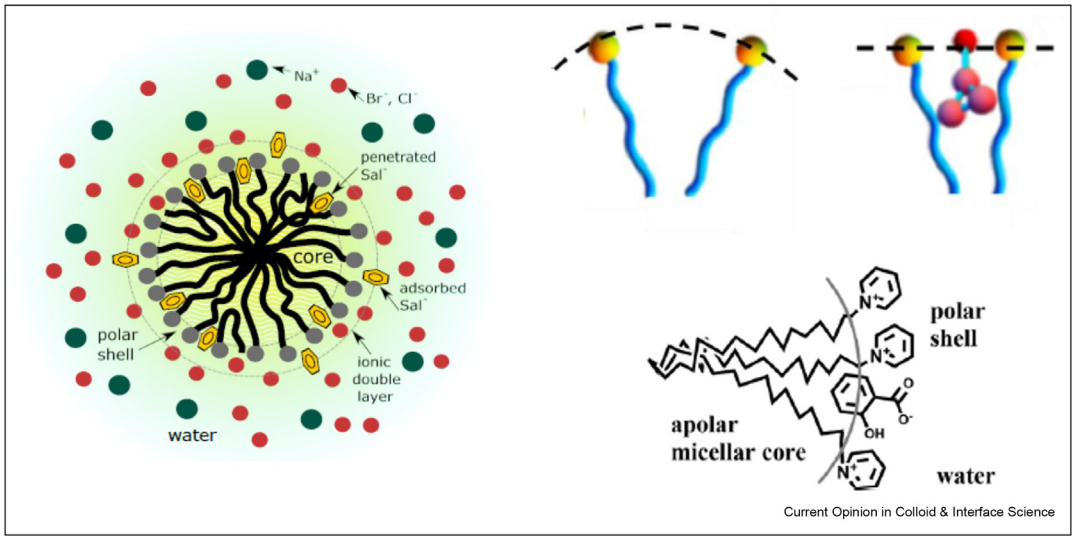

Possible interactions between the self-assembly of amphiphilic molecules dispersed in aqueous solutions and salts, adapted from Ref. [20].

characterization of WLMs, it remains a tricky technique, e.g. care should be taken during the blotting stage of the sample preparation due to a strong flow possibly applied to the WLMs, that can dramatically change their microstructure [27].

The conversion from linear to branched WLMs is often induced by a high salt content, accompanied by a reduction in the solution' zero shear viscosity, η_0. Figure 2 shows two examples of the viscosity trend coupled with very clear cryo-TEM images. The rheological and microscopic measurements have been performed on a surfactant solution at a fixed concentration of bis(hydroxyethyl)methylammonium chloride (EHAC) with a variable simple salt content (potassium chloride), Figure 2a, and on a solution containing 16.7 mM of cetylpyridinium chloride (CpyCl) and variable content of a binding salt (diclofenac sodium - NaDi), Figure 2b [5,28].

The viscosity drop has been justified from one side with an extra relaxation process (the low-cost-energy sliding motion of branch points along the main wormlike chain) [29] and on the other side with the wormlike micellar lengths reduction[24]. On top of this, it has been shown theoretically and experimentally [30,31] that an excessive increase of salt determines a decrease in the scission energy, which could cause a drop in average micelle length and viscosity.

Linear viscoelastic response and mesoscopic scales in WLMs

For most wormlike micellar solutions subject to small shear deformations, γ, shear stress relaxes like in the Maxwell model, $G(t) = G_0 \exp(-t/\tau_R)$ at long times, which corresponds to the behavior of the complex modulus $G^*(\omega) = [G'(\omega) + i\, G''(\omega)]$ at low and intermediate frequencies, ω, in the Fourier domain [32,33,34]. This viscoelastic spectrum can be measured by Small-Amplitude Oscillatory Shear (SAOS), and it has been intensively used to quantify micellar systems' viscoelastic features [35,34]. The elastic frequency independent plateaus modulus, G_0, can be directly evaluated from the experimental data; the relaxation time, τ_R, can be obtained from the intersection of $G'(\omega)$ and $G''(\omega)$ curves. When WLMs are long enough, they can entangle. There is evidence of sticky contacts between WLMs, which crosslink the WLMs and thus form a three-dimensional network [36]. When the micellar breaking and reforming process time is faster than the reptation time, a mean chain length dominates the relaxation process. It produces a decaying exponential stress relaxation, whose relaxation time is identical to the geometric mean of the mentioned characteristic times. Both relaxation times follow an Arrhenius-like dependence on temperature. A wide range of activation energies have been reported for WLMs (70−300 kJ/mol), which do not differ much from those of polymers in flow regimes (40−100 kJ/mol). For WLMs, the ratio τ_R/η_0, is a strong function of temperature, in contrast with unbreakable polymers, for which the ratio is a soft function of temperature. This strong dependence originates from both the decrease in the average micellar length and the increase of the scission rate constant when temperature increases [37].

To better describe the linear rheology of entangled WLMs, several improvements have been developed to

Figure 2

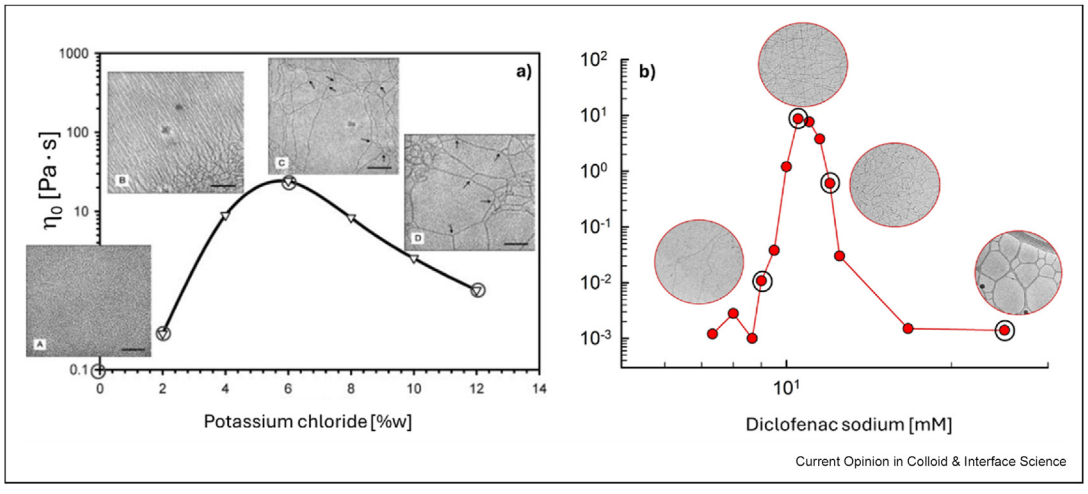

Zero shear viscosity as a function of salt content for two solutions, along with cryo-TEM images (images refer to the circled concentrations). **(a)** For a solution containing 1.5 % by weight of EHAC and different contents by weight of potassium chloride (readapted by Ref. [5]; **(b)** For a solution containing 16.7 mM of CPyCl and different content of NaDi (readapted by Ref. [28]).

include high-frequencies where other relaxation modes appear. Using the Poisson renewal approach, Granek and Cates [38,39] widened the basic reptation-only framework to include extra stress relaxation processes, such as the contour of length fluctuations and intra-tube Rouse modes. Other models have been developed to deal with WLMs linear rheology; a recent survey can be found in Ref. [40]. Lequeux [41] developed the concept of a population balance equation considering WLMs as a population of chains differing in length to produce a balance equation on stress, where self-assembling structures continuously exchange material. Both mass and stress of the original structures are transferred to a new segment of the wormlike micellar size distribution through stress balance terms attached to an existing stress relaxation differential constitutive equation (without rearrangement). This model has been improved by Peterson and Cates [42], using a simplified approximation of the population balance approach named *shuffling*.

The main ideas of Cates and the mentioned relaxation mechanisms have been incorporated with greater precision into the so-called "pointer algorithm", a mesoscopic simulation method, which gives an explanation of the disentanglement dynamics, the micellar reactions controlling the mean micellar length, and the structural flexibility of branched and linear WLMs [43–45]. This method developed by Larson's group includes reptation, micellar breakage/reforming, as well as fluctuations of contour length, and Rouse modes that are already included in Cates' model. Besides, this method involves constraint release, bending modes, and a cross-over to the tight entanglement regime. The procedure uses "pointers" that follow the ends of unrelaxed parts along each micelle, thereby permitting efficient simulations of the relaxation dynamics in a box containing abundant micelles in a way to obtain reliable results without neglecting correlation [44,46]. Very recently, the pointer algorithm's predictions were shown to match those of a microscopic slip-spring model that was validated against rheological data from polymers, too. This allows the estimation of mesoscopic length scales, eliminating a significant gap in the characterization of wormlike micellar solutions [47].

Mesoscopic scales play a crucial role in determining soft matter properties. In WLMs, they are related to the entangled micellar network, such as the average micelle total contour length, L_C, both persistence, l_p, and entanglement, l_e, micellar lengths, and the mesh size of the formed network, ξ. These parameters can be estimated from $G'(\omega)$ experimental data extended to high frequencies (see Figure 3), and they are given as input to mesoscopic simulations or theoretical models in a way to refine mesoscopic information; reviews of experimental methods can be found in [48]. The experimental data must cover a wide range in frequency, often obtained by combining rheological data with Diffusive Wave Spectroscopy (DWS) [30]. Rheology can rarely be used to evaluate all the characteristic micellar lengths by itself, although very recently, in very dilute wormlike micellar solutions, the whole relaxation spectra were covered by linear rheology [28]. Figure 3 shows experimental evidence of the high-frequency regime obtained through DWS measurements at different temperatures [30] or via rheological experiments in dilute solutions at ambient temperature [28]. The experiments shown in Figure 3 are performed on the same surfactant molecule (CPyCl), but with a different concentration and different salts.

Figure 3

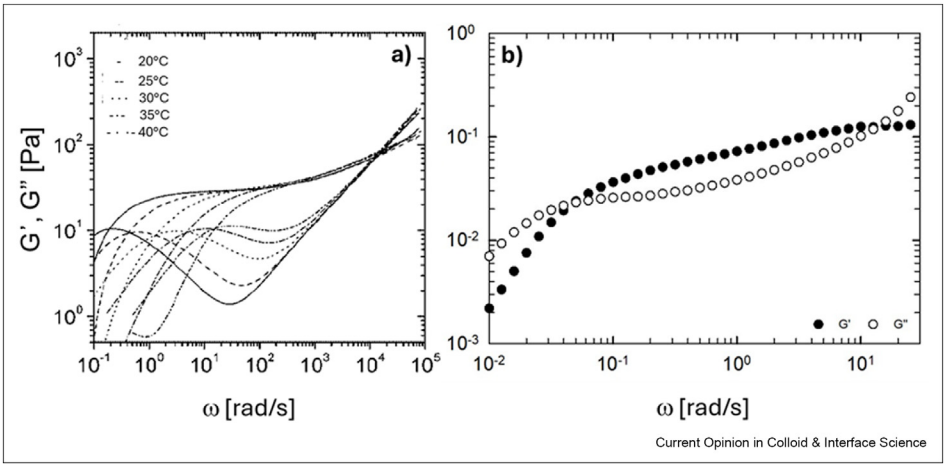

Dynamic shear moduli on surfactant solutions made of CpyCl. **(a)** DWS experiments at various temperatures were performed on 100 mM CpyCl/60 mM sodium salicylate (NaSal) solutions. Readapted from Ref. [30] **(b)** Frequency sweep test at 25 °C performed on 5 mM CPyCl, 4 mM NaDi. Readapted from Ref. [28].

Figure 4

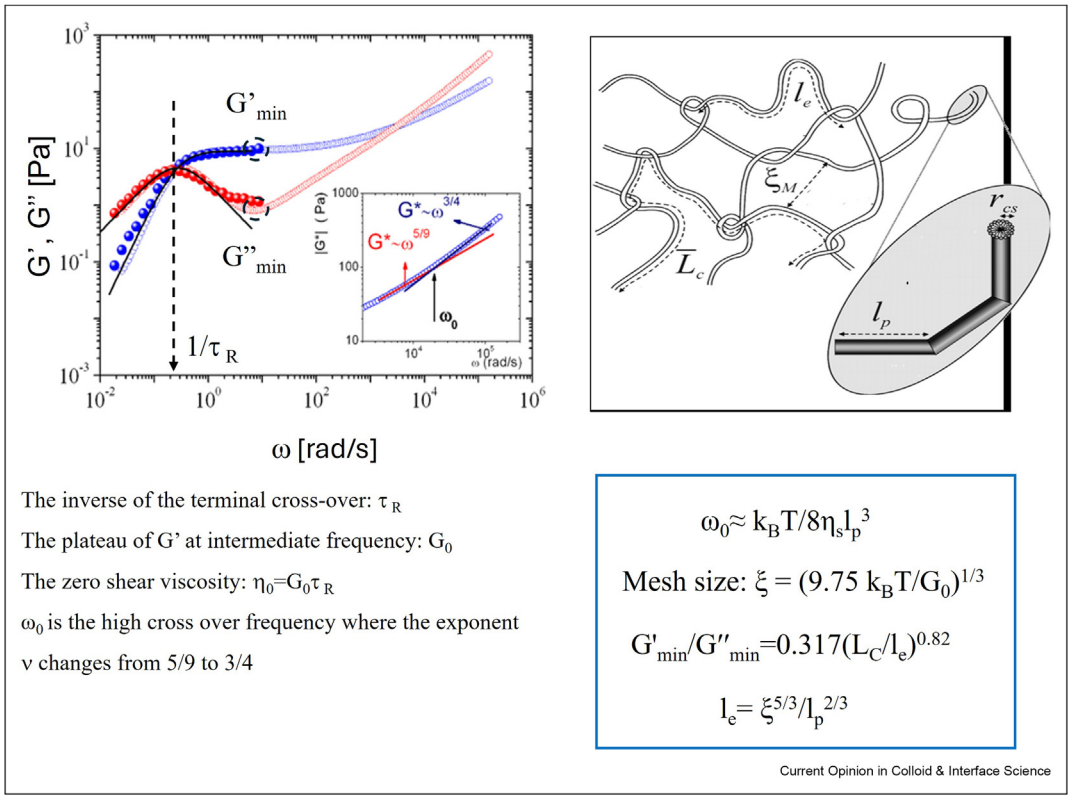

Mesoscopic scales, the formulae, and how to evaluate them from the viscoelastic spectra determined by SAOS and DWS. Comparison between rheometry data (full symbols – red G″, blue G′) and DWS (open symbols). The inset shows the complex modulus power laws at high frequencies. Readapted from Ref. [49] for the TDPS/SDS system.

At time scales shorter than the micelles' breaking time, WLMs act as flexible polymer chains [50], where stress relaxation is essentially governed by the Rouse-Zimm modes at not-so-high frequencies and by internal relaxation of Kuhn segments at higher frequencies. $G'(\omega)$ exhibits a power-law behavior, $|G'| \sim \omega^{\nu}$, with $\nu \sim 5/9$ corresponding to the Rouse-Zimm regime that changes to $\nu \sim 3/4$, when the internal bending modes of Kuhn segments are dominant; the boundary happens at a specific frequency ω_0 ($\omega_0 \approx k_BT/8\eta_s l_p^3$; η_s is the viscosity of the solvent) [51]. From this change of slope in $|G'(\omega)|$, l_p can be evaluated, as well as other characteristic lengths.

The wormlike micellar network mesh size can be estimated in the loose entanglement regime using $\xi = (A\, k_BT/G_0)^{1/3}$, where the coefficient $A = 9.75$ is a dimensionless prefactor, which includes correlations for loosely entangled polymers [45,37]. l_e can be estimated with $l_e = \xi^{5/3}/l_p^{2/3}$.[39]. Through incorporating breathing and high-frequency Rouse modes, the average total contour length can be calculated using $G'_{min}/G''_{min} = B\,(L_C/l_e)^{0.82}$. Here, the ratio G'_{min}/G''_{min} is evaluated at the frequency where G'' exhibits a local minimum, and G'_{min} is the value of the elastic modulus at the frequency where the local minimum in G'' appears; the exponent, usually equal to unity [35], is a correction derived by Granek, refining the estimate for the dip value G''_{min} [38]; the prefactor $B = 0.317$ has been recently evaluated by Larson and coworkers, by fitting to the predictions of the pointer algorithm [47]. The effort of correlating rheology with micelle lengths has often been hindered by the difficulty of accurately measuring these parameters, and their estimation usually needs fitting. Further steps are required to connect experimental measurements and modeling estimates depending on micelle lengths, salt concentration, and other additives, as well as their behavior in a nonlinear regime. We summarize the mesoscopic length scales, the formulae for their evaluation, and the connection with the viscoelastic spectra in Figure 4, where we also show the rheometry and DWS microrheology data for comparison.

Nonlinear behavior in WLMs and inertio-elastic instabilities

Many applications employing WLMs involve fast flows, which causes intriguing phenomena such as chain-scission, structure formation, and elastic instabilities [52]. When inertia is negligible, the Weissenberg number, expressed as $Wi = \tau_R/T_d$, is the control parameter, which denotes the elastic to viscous forces ratio, where T_d is a characteristic time for the deformation process. This definition implies a constant relaxation time, which does not change in nonlinear regime, although very recently, Rogers and coworkers showed that the relaxation times can be considered rate-dependent, with this approach being able to describe various aspects of WLMs rheology [53]. By keeping the *old-fashion* version of the Wi number, in the case of steady shear, $\mathrm{Wi} = \dot{\gamma}\ \tau_R$, with $\dot{\gamma}$ the shear rate. For oscillatory shear $T_d = 1/\ \dot{\gamma}_o = 1/(\omega\ \gamma_o)$, $Wi_0 = \omega\ \gamma_o\ \tau_R$ [54]. When $Wi < 1$, a linear response is expected. Constitutive equations properly adapted from the nonlinear response of linear entangled polymeric chains have successfully been used for WLMs, showing that entangled linear wormlike micelles, in some cases, appear to align, stretch, and tumble just like polymeric chains in startup flow when $Wi > 1$[50]. In some other cases, WLMs, submitted to a strong shear flow, can eventually show a structural nonlinearity which arises as an almost flat plateau in the shear stress, σ, versus shear rate, $\dot{\gamma}$, flow curve, where the fluid becomes dramatically shear-thinning, where the viscosity vs shear rate plot slope is ~ -1. They can show a non-equilibrium phase coexistence arising along the gradient direction between an isotropic solution and an aligned band (paranematic) with lower viscosity than the quiescent phase [4,55–58]. These bands result from mechanical instability, where the multivalued nonmonotonic constitutive curve presents a negative slope ($d\sigma/d\dot{\gamma} < 0$), producing two branches (shear bands) separated by a stress plateau to reach mechanical stability, one at low and another at high shear rates [55–57]. It is common that band sizes follow roughly an equality comparable to the lever rule. In other words, in a simple shear-banding scenario, the fluid is divided into just two clear regions separated by a thin, steady interface of very small width [59,60]. The paranematic phase high shear band presents birefringence related to the micellar orientational order. Neutron scattering confirmed the nematic distinctive mark of this phase [59,60]. The low shear band is made mostly of isotropic fluid.

In contrast to gradient banding, vorticity banding requires a single shear rate to support multiple shear stresses. This instability is observed in Couette flow as stacked bands along the vorticity direction (vorticity bands) [61,62] . Since some parts of the domain lie in regions of the flow curve where $\partial\sigma/\partial\dot{\gamma} > 0$, while others lie in the region where $\partial\sigma/\partial\ \dot{\gamma} < 0$ (σ *is* the shear stress), it produces a mixed behavior that can lead to complex flow instabilities in Couette flows as finger-like structures, unstructured streaks, and branches spanning along the gap, and vorticity bands. Hommel and Graham have studied these instabilities recently using the reformulated reactive rod model where micelles are described as rigid Brownian rods undergoing reversible scission and fusion in flow [63,64].

Although the simple scenario at steady state is somehow understood, coupled with the onset of shear-banding, a strong strain hardening in the transient regime is often detected, with a stress growth coefficient overcoming the Linear Viscoelastic Envelope (LVE) obtained from linear rheological data[65]. An example is reported in Figure 5. Very recently, the transient nonlinear rheological tests on a self-assembled wormlike micellar solution have been interestingly reviewed in terms of recoverable and unrecoverable strain [66], confirming that at low accumulated strain, the response is elastic in nature. At high strain, an anomalous increase in the stress growth coefficient sometimes appears in time, displaying a sudden inflection point. The stress growth coefficient, after the inflection point, occasionally remains below the LVE (see, for example, the blue line in Figure 5a, corresponding to $Wi = 3.2$). In all cases, when available, the stress growth coefficient passes through a sharp maximum before reaching a steady state. The value of the stress at long times is reported in Figure 5 b). Similarities are found in recent data on linear polymers [67] and on telechelic associating polymers [68].

In summary, it is assured that just after the peak (as shown in Figure 5), the system experiences a shear-banding transition, which develops over time before reaching its expected steady transition [69,70]. However, the foremost reason shear bands develop in these conditions is still under debate, as well as the hysteresis in the up-shear and down-shear flow curves related to this strain hardening. However, recent measurements show that when the measurement time in each measurement is much larger than the relaxation time, all hysteresis in the shear flow curves is reduced [71]. When the elastic contribution in wormlike systems is high, the simple shear-banding scenario does not occur, and multiple bands can be commonly detected [71].

Simple fluids at high shear flow can be unstable and ultimately turbulent due to inertia when the Reynolds number, $Re = \tau_1\ \dot{\gamma}$, increases, where $\tau_1 = \rho d^2/\eta_0$ is the viscous diffusion time; here d, η_0 and ρ are a characteristic length in the velocity gradient direction, the viscosity, and the mass density, respectively. In Taylor-Couette flow with a small gap between the cylinders (d), Taylor illustrated that the purely azimuthal base flow turns out to be unstable when the Taylor number $Ta_i = \Lambda^{1/2} Re$ increases over some critical value. Here, Λ

Figure 5

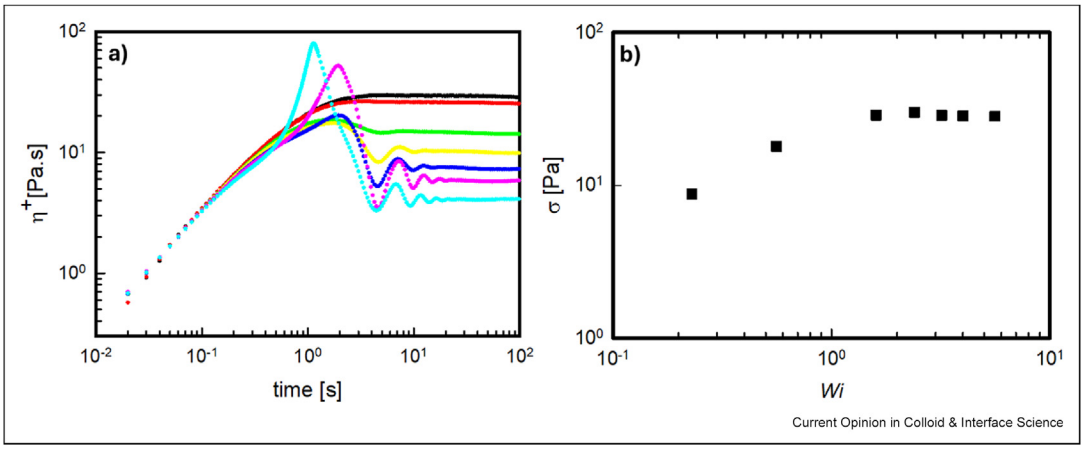

(a) Stress growth coefficient in startup flow at different shear rates performed on wormlike micellar solution containing 100 mM CPyCl and 67 mM NaSal. Different colors correspond to different *Wi* values: black 0.23; red 0.56; green 1.6; yellow 2.4; blue 3.2; pink 4; cyan 5.6. **(b)** Steady-state value of the stress (obtained from data at long times in a)) *vs Wi*. A flat plateau appears when $Wi > 1$, denoting the presence of a shear-banding phenomenon.

$= d/R_i << 1$ denotes the streamlines dimensionless curvature, with the inner cylinder of radius R_i rotating. Another route to instabilities occurs due to the additional time scale in WLMs, i.e., the relaxation time τ_R that does not involve inertia and is purely elastic. Nonlinear experiments can probe the interval between the steady-states and strongly time-dependent behaviors, discovering the consequence of varying the dynamic variables: the Deborah number, *De*, and the Weissenberg number, *Wi*. Here, we defined the Deborah number ($De = \tau_R\omega$) as the ratio of a characteristic relaxation time of a material, τ_R, and a characteristic time scale of the deformation process observation, $T = 1/\omega$. By coupling neutron scattering and shear rheology, Lee et al. recently discussed the possibility of describing both linear and nonlinear rheology with the magnitude of the recoverable strain [72]. Although the idea is new and surely challenging, we decided to focus on literature data reviewed in terms of the applied strain, for a matter of simplicity. A linear response is anticipated when the applied strain is slight or when $Wi << 1$. When $De << 1$ a reconfiguration dynamic is expected that keeps up with the applied deformation, leading to a quasi-steady state response where the stress slowly goes up and down along the steady-state flow curve and the shear rate varies through a cycle. In comparison, when $De >> 1$, the system's relaxation dynamics is not able to follow the applied deformation and an elastic-type response would be expected. If $Re << 1$, then the *Wi* number is the control parameter that may cause the appearance of secondary flows and, ultimately, to elastic turbulence [73]. Homogeneous flow becomes unstable when $Ta_i = \Lambda^{1/2}Wi$ surpasses a particular value. However, it is imperative to note that the appropriate dimensionless group for purely elastic instability comes from the band with high shear rate [73]. Flow instabilities are denoted as inertio-elastic when both *Re* and *Wi* are large. A precise instability scaling is not known, even for the Taylor-Couette geometry. By dimensional analysis, it has been proposed that the Taylor number should be expressed as a function of Re and *Wi*, $Ta = \Lambda 1/2\, f(Re, Wi)$. When $\mathcal{E} \to 0$, *f* goes to *Re*, and when $\mathcal{E} \to \infty$, *f* goes to *Wi*. Here, $\mathcal{E}$ *is* the ratio of elastic to inertial forces in a fluid, named as the elasticity number, $\mathcal{E} = Wi/Re = \tau_R/\tau_1$ [54,74].

Wormlike micellar solutions present purely elastic instabilities when inertia is negligible, as in other viscoelastic fluids[75]. Shear-banding instabilities produce vortex flows confined to the high shear flow band[73]. The banding-structure formation kinetics and the spatiotemporal fluctuations, reminiscent of the Taylor-like instability detected in viscoelastic polymeric solutions, have been thoroughly studied in WLMs [73,76]. In this case, shear-banding instabilities produce vortex flows confined to the high shear flow band [77]. The banding-structure formation kinetics and the spatio-temporal fluctuations reminiscent of the Taylor-like instability detected in viscoelastic polymeric solutions have been thoroughly studied [73,76]. The band interface undulates due to an underlying secondary vortex flow, primarily localized in the high *Wi* band. The image of two stable shear bands separated after the onset of the shear-banding, *i.e.*, at $Wi \geq 1$, by a steady interface, has many theoretical challenges[74,78], which promoted the exploration of elastic instability mechanisms as the potential source of triggering secondary flows, that are considered responsible for the fluctuations on the main flow. When there is no stress diffusion, linear stability for shear-banding in a planar Couette flow shows that flow is unstable for most arrangements of two

bands for long waves, employing the Johnson-Segalman model fluid [79]. A slight stabilizing effect is present in the case of weak diffusion, although the primary long-wave instability mechanism is not really modified. Starting at the onset of secondary flows, which is localized in the high shear rate band, follows a deformation of the interface between bands, and the evolution of the secondary flow depends on the boundary conditions of the unstable domain (hard or soft). The existence of the three distinct scenarios has been experimentally confirmed [73], and a dimensionless criterion to rationalize the onset of these secondary flows in the base shear-banding flow of WLMs has been established [80]. Other instability mechanisms of elastic origin have been studied, and it has been suggested that the jump in normal stress between bands could generate interfacial modes. The spatiotemporal dynamics for secondary flows is not yet fully understood since the control parameter is still not explicit for transitions between spatiotemporal dynamics. Examples of spatiotemporal dynamics classes of secondary flows inferred from the evolution of the position of the interface between bands during a step in shear rate from rest have been noticed [73]. On the other hand, there are reports of non-shear-banding (homogeneous) WLMs where inertia is significant in which flow patterns analogous to those in the inertio-elastic regime of dilute polymer solutions appear, following a sequence: CF (Couette Flow)/SV (Standing Vortex)/DRSW (Disordered Rotating Wave Pattern)/EDT (Elastic Dominated Turbulence)[81].

Nonlinear effects occur if the strain amplitude increases, as exemplified by LAOS.[54]. A sinusoidal strain-imposed protocol is used, expressed as $\gamma = \gamma_0 \sin\omega t$, where γ_0 is now a large strain amplitude, ω is the frequency, and a derivative can evaluate the shear rate $\dot{\gamma}(t) = (\gamma_o\omega)\cos\omega t = \dot{\gamma}_o \cos\omega t$. Meanwhile, the response to stress by viscoelastic complex fluids is independent of the shear direction; therefore, the nonlinear shear stress can only be represented by odd harmonic contributions. After an initial transient, the system's response achieves a time-translationally invariant state from cycle to cycle. Explicitly, changes in shear stress due to higher harmonics contribution can be visually observed through the Lissajous-Botwich (LB) curves, which are 3D curves (σ/σ_o *vs.* γ/γ_o and $\dot{\gamma}/(\gamma_o\omega)$) and by their projections (elastic representation: σ/σ_o *vs.* γ/γ_o or viscous representation: σ/σ_o *vs.* $\dot{\gamma}/(\gamma_o\omega)$)[54]. An example of a micellar solution made of CTAB/NaSal at different Wi_0 and De is presented in Figure 6, which is called a Pipkin diagram. A distinctive characteristic of LAOS in Maxwellian fluids is that the severity of the flow's time dependence, relative to the fluid's relaxation τ_R, can be adjusted by varying ω in the applied strain but without abrupt jumps in the strain input, as occurs in step experiments[54]. Therefore, for WLMs following the Maxwell model under strain-imposed protocol in a LAOS experiment, if the applied strain is minimal, $\gamma_o << 1$, as in SAOS, the shearing strain amplitude can be expressed as $\gamma_0 = Wi_0/De$ and the angular frequency by $\omega = De/\tau_R$. Then, the shear stress, $\sigma(t)$, can be described by $\sigma(t) = (Wi_0/De)[G'\sin(De/\tau_R)t + G''\cos(De/\tau_R)t]$; here $G' = G_0\,[De^2/(1+De^2)]$ and $G'' = G_0\,[De/(1+De^2)]$. The loci of $\sigma(t)$ *vs.* $\gamma(t)$ is an ellipse determined by $\sigma^2 - 2G'\sigma\gamma + (G'^2 + G''^2)\gamma^2 = [G''\,Wi_0/De]^2$; the stress maximum occurs in the first quadrant, i.e., where variables are positive, of a σ *vs.* γ graph ($\sigma^{max} = \gamma\,[(G'^2 + G''^2)/G']$). However, since LAOS is not restricted to γ_o small, the response of WLMs to oscillatory shear strain can be explored by selecting large γ_o, which produces large deviations from the linear performance. For a fixed Wi_0, when $De >> 1$, WLMs can exhibit a nonlinear elastic response at ω with periods shorter than the time scale needed to form a shear band. When $De << 1$, this flow produces a quasi-steady state response, where stress repeatedly sweeps up and down as the shear rate changes through a cycle.Time-resolved small-angle neutron scattering t-SANS [82] identified the different frequency regimes where measurements were almost equal to the expectations given by the Maxwell model in the linear regime.

Shear-banding in LAOS has been experimentally observed [82], and a few models have been capable of predicting shear banding. For instance, those employing the partially extending convected (PEC) equation [83], or the Vasquez–Cook–McKinley model [45]. Nevertheless, to determine shear-banding theoretically, models must include nonhomogeneous flow and a criterion for the shear-banding onset. Considering that the underlying stress constitutive curve, a function of strain rate, is nonmonotonic, it is insufficient [84]. The Rolie-Poly (RP) model used for the case of polymers and WLMs has been considered for the shear band formation in LAOS [85] with some success. Here, a single-mode approach has been assumed to consider just one reptation relaxation timescale and one elasticity relaxation timescale. Then, shear-banding appears for monotonic constitutive curves. Chain rupture and recombination narrow the relaxation spectrum, so this single-mode approach can provide an entire image of the parameter space. Therefore, shear-banding is considerable, and the mechanisms that generate its onset can be identified, allowing it to focus on understanding the shapes of the stress curves versus strain or strain rate. The Lissajous plots have been considered as the result of a sequence of physical processes and have linked to a molecular origin of a Kuhn segment scale and elasticity[86].

However, it is not easy to understand the physical meaning of all changes in LB curves. Comprehensive frameworks have been developed to better describe and understand the nonlinear viscoelastic response from an imposed deformation protocol applied to WLMs. Here, we will describe just two of the most distinctive procedures. The Chebyshev decomposition method

Figure 6

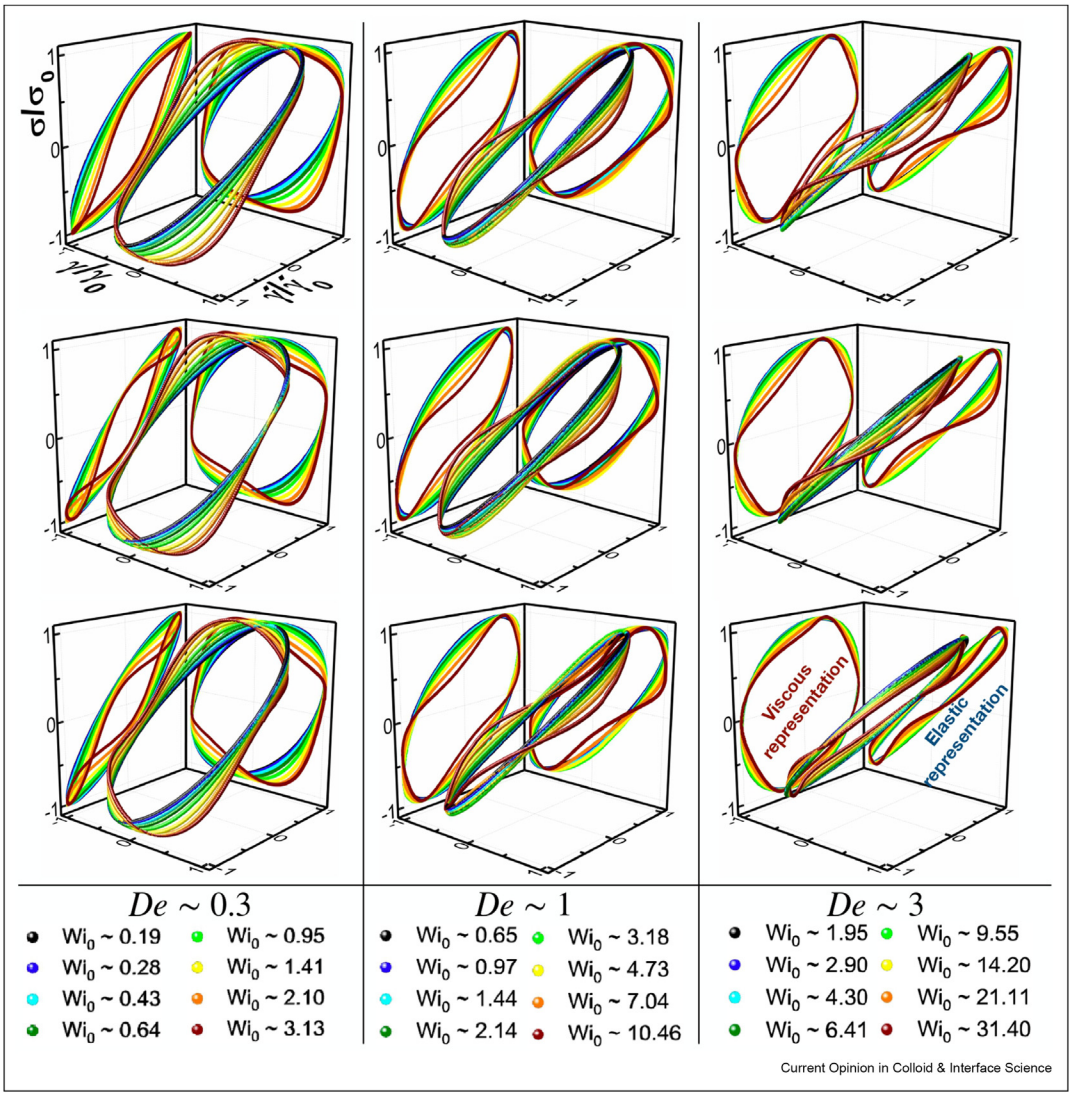

Normalized 3D Lissajous-Bowditch curves and projections (elastic representation: σ/σ_o *vs.* γ/γ_o or viscous representation: σ/σ_o *vs.* $\dot{\gamma}/(\gamma_o\,\omega)$) for a micellar solution made of CTAB/NaSal ([NaSal]/[CTAB] = *4*, and *[CTAB] = 0.1 M*), using different Wi_0 ($=\tau_R\omega\,\gamma_o$) and *De* ($=\tau_R\omega$). The temperature from the upper row to the lower one is *T = 20, 25,* and *30* °*C*, respectively. Figure taken from Ref. [71].

(TDM), where the stress is decomposed into a sum of contributions dependent on the strain (elastic stress) and the strain rate (viscous stress), provides global and local measures at specific points. Quantitative material functions are calculated just using the total strain; physical interpretation of the material responses is obtained based on the signs and magnitudes of these material functions.

On the other hand, the sequence of physical process method (SPPM) analyzes the transient material responses by tracking the trajectory of the stress responses instantaneously as a function of both the strain and the strain rate. This framework describes the three-dimensional Lissajous figures providing instantaneous (local) elastic and viscous responses throughout the oscillation cycle and global measures, and it makes use of the decomposed strain into recoverable and unrecoverable strains that can be obtained experimentally. In particular, the loss modulus, related to the average dissipated energy during the oscillation, is a composite parameter that can be split into contributions from recoverable and unrecoverable strain rates representing the viscoelastic solid- and liquid-like behaviors. At the end of the examination, the TDM, which is based on the total strain and total strain rate, describes the material responses by one elastic and one viscous property. In contrast, the SPPM provides one recoverable elastic and

two viscous properties, allowing for a more explicit interpretation of the nonlinear behavior. Therefore, a problem usually treated as a mathematical problem can be solved experimentally by acknowledging the extra information provided by recovery rheology. Quite recently, both methods have been confronted by Shim and coworkers [87]. These authors show that the two methods provide competing physical interpretations when derived from the total strain but provide unified interpretations when decomposed strains describe them.

The TDM description assumes a sinusoidal shear strain and a cosinusoidal strain rate. The resulting stress is described as the sum of two contributions, elastic stress σ' and viscous stress σ". The decomposed stresses is represented in terms of orthogonal Chebyshev polynomials:

$$\sigma' = \gamma_0 \sum_{n=odd} e_n(\omega, \gamma_0) T_n\left(\frac{\gamma}{\gamma_0}\right) \quad (1)$$

$$\sigma'' = \dot{\gamma}_0 \sum_{n=odd} v_n(\omega, \gamma_0) T_n(\dot{\gamma} / \dot{\gamma}_0) \quad (2)$$

Here, T_n is the nth-order Chebyshev polynomial of the first kind, e_n (ω, γ_0) and v_n (ω, γ_0) are the elastic and viscous Chebyshev coefficients, respectively, which are independent of each other. In this method, the third harmonic elastic and viscous Chebyshev coefficients are essential to interpret the nature of the nonlinearities where the stress−strain relation is no longer describable by linear differential equations with constant coefficients, and the Lissajous curves are distorted. Therefore, new parameters to capture intracycle nonlinearities must be introduced to determine the local behavior of graphs of stress *vs.* strain or *viceversa*, as the local moduli and local viscosities within a cycle at specified points, which can be evaluated with the Chebyshev coefficients to quantify intracycle nonlinearities, distorting the linear viscoelastic ellipse. Subsequently, it is necessary to define the strain-stiffening ratio (S) and shear-thickening ratio (T) introduced by Ewoldt et al. [88] defined as $S = \frac{G'_L - G'_M}{G'_L}$ and $T = \frac{\eta'_L - \eta'_M}{\eta'_L}$; these quantities can be evaluated by the coefficients of the Chevychev expansion. Here, G'_M is the minimum-strain modulus or tangent modulus at $\gamma = 0$, G'_L is the large-strain modulus or secant modulus evaluated at the maximum strain, η'_M is the minimum-rate viscosity, and η'_L is the large-rate viscosity. Now, TDM arrives to the rheological response of materials, which are linear when $S = 0$ and $T = 0$. When $S > 0$ and $T > 0$ materials are strain-stiffening and shear-thickening in the intracycles. For the case of negative values, $S < 0$ represents strain-softening and $T < 0$ shear-thinning in intracycles.

In contrast, SPPM permits a dynamic interpretation via defining a transient modulus and viscosity within an oscillation, presenting a response trajectory in the space defined by the strain, strain rate, and stress without assuming any shear symmetry as TDM needs. These instantaneous modulus, $G_t(t)$, and viscosity $\eta_t(t)$, result in the partial derivatives of the stress with respect to the strain and rate, respectively, and they can be interpreted depending on the relative magnitudes and their derivatives. In this way, the transient response will be stiffening or softening when the instantaneous modulus increases or decreases at a given instant. In the same form, when the instantaneous viscosity increases or decreases, the transient response is interpreted as thickening or thinning. Considering now that the strain can be decomposed into recoverable and unrecoverable strains experimentally, i.e., $\gamma(t) = \gamma_{rec}(t) + \gamma_{unrec}(t)$, the SPPM parameters can be rewritten in the form of the recovery rheology perspective, producing an equation for $\sigma(t)$ in terms of Chebyshev polynomial of the first kind and the recoverable and unrecoverable strains $\gamma_{rec(t)}/\gamma_{0,rec}$ and $\dot{\gamma}_{rec(t)}/\dot{\gamma}_{0,rec}$ (substituting the unrecoverable strain from the recoverable strain expressions in the last equation). Here, the zero subindex in γ_0 and $\dot{\gamma}_0$, corresponds to the maximum values of the recoverable strains or recoverable strain rates. The Chebyshev coefficients following a similar notation as in (1) and (2) allow to define new material functions in terms of recoverable and unrecoverable strains in the SPPM: ${}^{rec}e_1$, ${}^{rec}v_1$, ${}^{rec}e_3$, ${}^{rec}v_3$, and ${}^{unrec}v_1$,${}^{unrec}v_3$. This leads to the recovery rheology to provide two newly local moduli, ${}^{rec}G'_M$ and ${}^{rec}G'_L$, and four local viscosities (${}^{rec}\eta'_M$, ${}^{rec}\eta'_L$, ${}^{unrec}\eta'_M$, and ${}^{unrec}\eta'_L$) all in terms of these mentioned Chebyshev coefficients. These functions produce a more detailed interpretation of a response of a wormlike micellar fluid: If ${}^{rec}G'_L, > {}^{rec}G'_M$, strain stiffening; ${}^{rec}G'_L < {}^{rec}G'_M$, strain softening; ${}^{rec}\eta'_L > {}^{rec}\eta'_M$, rate thickening; ${}^{rec}\eta'_L < {}^{rec}\eta'_M$, rate thinning; ${}^{unrec}\eta'_L > {}^{unrec}\eta'_M$, rate thickening; ${}^{unrec}\eta'_L < {}^{unrec}\eta'_M$, rate thinning. As described, the SPPM depends on the recovery rheology and produces two different response trajectories defined by the recoverable and the unrecoverable components, allowing a better interpretation of material responses. Shim et al. [87] describe the conditions where the TDM gives the same results as SPPM and under what circumstances caution should taken when TDM interpretations are used. The use of recovery rheology provides more information than TDM and allows more detailed interpretations; apparently, SPPM accurately represents the physics of materials. In particular, a cetylpyridinium chloride/NaSal micellar solution was studied with SPPM by Shim et al., and the results are shown in their supplementary material section [87].

Besides shear deformation, WLMs have revealed rich dynamics in extension, although this flow type has received far less attention than shear. Moreover, recent studies have shown that uniaxial extensional rheology could be able to discern between linear and branched

self assemblies [52,89,90]. The extensional behavior of WLMs was initially studied with four roll mills and opposite jet devices [91,92]. These devices are, nevertheless, unable to make transient rheological measurements and are affected by an unknown pre-strain history. Prud'homme and Warr studied the response of various wormlike micellar solutions, and they found that above a critical value of the extensional rate, the solutions showed a maximum in viscosity followed by a sudden drop with a hint of birefringence. They discussed that micelles can undergo scission when the extensional flow is strong enough, which was later supported by other experiments performed with opposed jet devices [93]. More recently, the Capillary Breakup Extensional Rheometer (CaBER) [94] and the Filament Stretching Rheometer (FiSER) [95] have been used to measure the response of wormlike micellar solutions to an imposed transient homogeneous uniaxial extensional flow field, by monitoring the filament thinning and the subsequent pinch-off process. In particular, the CaBER can measure very low apparent extensional viscosities, relaxation times, and reach extremely high Hencky strains [96]. Recently introduced by Dinic and co-authors [97], the dripping-onto-substrate (DoS) extensional rheometry has addressed some shortcomings of the CaBER technique, enabling the characterization of low-viscosity, low-elasticity, and low surface tension WLMs [98]. Recently, a modified Temperature-Controlled DoS (TC-Dos) was introduced [69]. A single droplet is gradually extruded from a nozzle and contacts a substrate, forming a liquid bridge that undergoes capillary-driven thinning and breakup (with a measurable - but uncontrolled - extensional rate). The absence of the step-stretch present in the CaBER technique allows a better evaluation of the micelle parameters. Figure 7 compares snapshots of the same WLMs measured with CaBER and DoS.

Thanks to these recent measurements, a consistent amount of data demonstrated that the extensional relaxation time, τ_E, obtained by fitting the stretching profile of the filament diameter over time, could be significantly smaller than the shear relaxation time, τ_R, in a wide range of WLMs (see Figure 7) [89,90,99]. A few works have been devoted to understanding the possible reasons for such a difference. The most accomplished one deals with micellar chain scission, which may lead to $\tau E/\tau R < 1$. Indeed, unlike polymers, which require energies of *100's* of k_BT to result in the macromolecule's scission energy, a wormlike micelle is expected to require only a few k_BT [100]. However, the scission energy evaluated in equilibrium conditions could differ from that in a strong applied flow. The micellar chain scission has been confirmed by light scattering devices [101], and its extent has been demonstrated to depend on the extensional fixture and

Figure 7

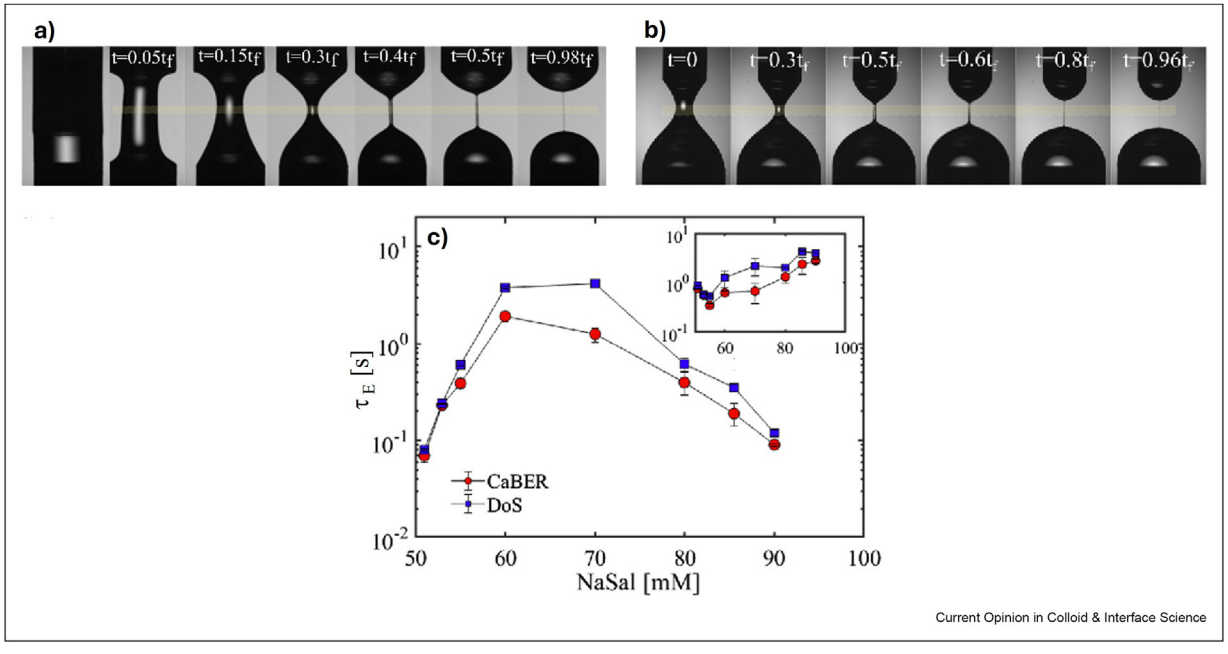

Snapshots showing the filament thinning process in the CaBER experiments **(a)** and in the DoS experiments **(b)** for a solution containing 100 mM CPyCl and 90 mM NaSal. The time t_f corresponds to the instant of filament pinch-off (t = 0.4t_f in a) and t = 0.5t_f in b)). **(c)** extensional relaxation time, τ_E, derived from the study of the thinning filament as a function of the NaSal concentration for a surfactant system containing 100 mM CPyCl, measured with CaBER and DoS. The inset reports the ratio τ_E/τ_R *vs* NaSal concentration. Figures readapted from Ref. [99].

the abruptness with which WLMs are subjected to uniaxial extensional flow [99]. A complete understanding of the failure mechanism for WLMs in a pure extensional flow is still needed, which could, for example, explain the absence of a turbidity variation in the fluid filament or a change in the birefringence signal when scission occurs.

Wormlike micelles' flow has also been studied in complex geometries, such as cross-slot and contraction expansion [102,103]. Although micelles always show a wide variety of interesting flow phenomena, the combination of extension and shear deformation in these geometries makes the data analysis less immediate.

Finally, microfluidic devices provide a versatile mode to study wormlike micellar solutions under various flow conditions. Zhao et al. [104] studied WLMs in confined microfluidic geometries, Stone et al. [105] imaged individual WLMs and measured its dynamics, Salipante et al. [106] studied jetting flow instabilities and the resulting velocity profiles, Singh et al. [107] took advantage of the WLMs micron-length scales and the possibility of reaching very high deformation rates in micro-electro-mechanical systems. Microfluidics has also been used to generate new microstructures, such as Flow-Induced Structured Phases (FISP), and to study new flow phenomena in WLMs [108,109].

Mesoscopic lengths to understand wormlike micellar rheology in nonlinear regime

The WLMs mesoscopic scales have recently been shown to help understand nonlinear properties ([50], p. 202; [65,110]). As mentioned, for $Wi > 1$, elastic forces are stronger than viscous forces. When the flow is slow, the disentanglement process can take place along the micellar network, moderately contributing to the elastic forces. In contrast, if the micellar network is quickly deformed, not permitting enough time for micelles to disentangle - due to the hastening of the imposed strain - the network's contribution to the tangled elastic forces rises because chains are stretched, losing conformation degrees of freedom, so entropy decreases, and a significant forces is required to avoid this decrease. The degree of entanglement of the micellar network responsible for elastic forces is considerable. The mean micellar contour length ratio to the average entanglement length is a property that could quantify the number of entanglements that occur in a micellar network. An entanglement index, $\kappa = L_c/l_e$, has been defined [71]. A wormlike micellar CTAB solution prepared to span many $\mathcal{E}$ ($=Wi/Re$) values along several decades ($\sim 10^{-1}$-10^{6}) showed that as κ increases, $\mathcal{E}$ increases almost linearly, but in two regimes with different slopes, forming a shoulder at $\kappa \sim 10$. However, theoretical developments are needed to comprehend the relation between $\mathcal{E}$ and κ. For example, since the physicochemical parameters of micellar solutions as well as the geometry of the elements forming the WLMs determine the mesoscopic scales at equilibrium, *Are the nonlinear instabilities in WLMs determined by these mesoscopic scales?* micellar solutions with large κ cannot disentangle efficiently- *Why are they linearly related to the elasticity number* $\mathcal{E}$? other mesoscopic scales also change, but *Why do they not impact the rheological behavior as* κ?

The precise disentanglement mechanisms are still unidentified; this is a challenge to understand WLMs dynamics adequately. Moreover, in LAOS and extensional experiments, κ cannot be evaluated along the deformation steps with the present state of our knowledge because experiments are far from equilibrium. Indeed, nowadays, κ is obtained very close to equilibrium conditions and could be, instead, strongly flow-dependent.

Conclusions

WLMs can be easily formulated experimentally with different viscosities using diverse surfactants and additives. Cryo-EM imaging still remains the easiest way to visualize WLMs in solution. The micelle scale lengths cannot be evaluated directly due to the strong deformations involved in sample preparation; new experimental methods would be welcome.

We reviewed experimental evidence and theoretical/modeling approaches to understand the wormlike micellar dynamics in linear and nonlinear regimes. In the last regime, much research needs to be done. Characteristic micellar length scales are challenging to measure and control via experiments, often requiring fitting a rheological model to obtain these length estimates; this has been a vibrant research area in the last decades. Although evaluated in equilibrium conditions, *i.e.* when a small deformation is applied, these parameters can be helpful to understand nonlinear phenomena encountered in fast flows, which are not yet fully explained. A few examples have been mentioned in this review, both in shear and extensional flows. Of course, the ability to link linear and nonlinear rheology with a priori formulation would be highly desirable to guide the design of WLMs, which have many implications in a wide range of industrial requests. We also explored the possibilities of LAOS to understand the WLMs' behavior through the Lissajous-Botwich curves. We described the most distinctive procedures to analyze them: the Chebyshev decomposition and the sequence of physical process methods. In the first method, the stress is decomposed into contributions dependent on the strain and the strain rate and, in the second one, the strain is decomposed into the recoverable and unrecoverable strains, which can be obtained experimentally. The use of recovery rheology provides information to give a more detailed interpretation of the material rheological

response than when the Chebyshev decomposition is used, providing a better description that accurately represents the physics of materials.

We limited our discussion to the simplest WLMs based on ionic surfactant molecules in aqueous solutions. Nevertheless, there are other ways to obtain WLMs, for example, from amphiphilic block copolymers [111,112]. For these systems, it is common that the linear viscoelastic spectra do not follow the Maxwell model due to their slower dynamics, driven by reptation, making their study even more complicated [113]. Another recent research line is to develop intelligent responsive WLMs that actively self-assemble in the presence of an external stimulus. The switching of micellar assembly structures has been reported using electrical, optical, thermal, or pH triggers, which can be used to modify the rheological response of solutions with embedded intelligent WLMs and their consequent mesoscopic length scales [16].

Declaration of competing interest

The authors declare that they have no known competing financial interests or personal relationships that could have appeared to influence the work reported in this paper.

Acknowledgments

RP thanks Nino Grizzuti and Dganit Danino for useful discussions. RP acknowledges TA Instruments for the Distinguished Young Rheologist Award 2018. RC acknowledges the DGAPA-UNAM Funding (IN104024).

Data availability

Data will be made available on request.

References

Papers of particular interest, published within the period of review, have been highlighted as:

* of special interest
** of outstanding interest

1. Davoodi S, Al-Shargabi M, Wood DA, Rukavishnikov VS: **A comprehensive review of beneficial applications of viscoelastic surfactants in wellbore hydraulic fracturing fluids**. *Fuel* 2023, **338**, 127228, https://doi.org/10.1016/j.fuel.2022.127228.

2. Goyal G, Elfring GJ, Frigaard IA: **Rheology and flow studies of drag-reducing gravel packing fluids**. *Rheol Acta* 2017, **56**: 905–914, https://doi.org/10.1007/s00397-017-1041-0.

3. Chu Z, Dreiss CA, Feng Y: **Smart wormlike micelles**. *Chem Soc Rev* 2013, **42**:7174–7203, https://doi.org/10.1039/C3CS35490C.

4. Cates ME, Fielding SM: **Rheology of giant micelles**. *Adv Phys* 2006, **55**:799–879, https://doi.org/10.1080/00018730601082029.

5. Dreiss CA: **Wormlike micelles: where do we stand? Recent developments, linear rheology and scattering techniques**. *Soft Matter* 2007, **3**:956–970, https://doi.org/10.1039/B705775J.

6. Nagarajan R, Ruckenstein E: **Theory of surfactant self-assembly: a predictive molecular thermodynamic approach**. *Langmuir* 1991, **7**:2934–2969, https://doi.org/10.1021/la00060a012.

7. Larson RG: *The structure and rheology of complex fluids*. New York (N.Y.): Oxford University Press; 1999.

8. ** Scigliani A, Grant SC, Mohammadigoushki H: **Probing self-assembled micellar topologies via micro-scale diffusive dynamics of surfactants**. *J Colloid Interface Sci* 2023, **642**: 565–573, https://doi.org/10.1016/j.jcis.2023.03.102.
The potential use of the noninvasive H NMR diffusometry to monitor the self-diffusion dynamics of individual surfactants and the relative topological transitions in micelles was investigated, overcoming challenges associated with traditional techniques.

9. Mukerjee P, Mysels K: ***Critical micelle concentrations of aqueous surfactant systems***. https://doi.org/10.6028/NBS.NSRDS.36.

10. Perinelli DR, Cespi M, Lorusso N, Palmieri GF, Bonacucina G, Blasi P: **Surfactant self-assembling and critical micelle concentration: one approach fits all?** *Langmuir* 2020, **36**: 5745–5753, https://doi.org/10.1021/acs.langmuir.0c00420.

11. Abooali D, Soleimani R: **Structure-based modeling of critical micelle concentration (CMC) of anionic surfactants in brine using intelligent methods**. *Sci Rep* 2023, **13**, 13361, https://doi.org/10.1038/s41598-023-40466-1.

12. Dan N, Safran SA: **Junctions and end-caps in self-assembled non-ionic cylindrical micelles**. *Adv Colloid Interface Sci* 2006, **123–126**:323–331, https://doi.org/10.1016/j.cis.2006.05.027. Special Issue in Honor of Dr. K. L. Mittal.

13. Wand CR, Panoukidou M, Del Regno A, Anderson RL, Carbone P: **The relationship between wormlike micelle scission free energy and micellar composition: the case of sodium lauryl ether sulfate and cocamidopropyl betaine**. *Langmuir* 2020, **36**:12288–12298, https://doi.org/10.1021/acs.langmuir.0c02210.

14. Zhang Y, Han Y, Chu Z, He S, Zhang J, Feng Y: **Thermally induced structural transitions from fluids to hydrogels with pH-switchable anionic wormlike micelles**. *J Colloid Interface Sci* 2013, **394**:319–328, https://doi.org/10.1016/j.jcis.2012.11.032.

15. Lv D, Liu Q, Wang C, Wu H, Zhao N, Yin B, Wei X, Li J: **Imparting pH and temperature dual-responsiveness in a micellar solution of cationic surfactants by introducing a hydrotrope**. *Soft Matter* 2022, **18**:5249–5260, https://doi.org/10.1039/D2SM00509C.

16. * Jora MZ, de Souza RN, da Silva Barbosa M, Speglich C, Sabadini E: **Rheological modulation of a pH-responsive wormlike micelle driven by charge and cosurfactant**. *J Mol Liq* 2024, **400**, 124512, https://doi.org/10.1016/j.molliq.2024.124512.
A fine experimental study was reported on responsive wormlike micelles obtained by tuning PH, with very clear cryo-TEM pictures.

17. * Gonçalves RA, Holmberg K, Lindman B: **Cationic surfactants: a review**. *J Mol Liq* 2023, **375**, 121335, https://doi.org/10.1016/j.molliq.2023.121335.
A comprehensive review on the self-assembly, intermolecular interactions, and properties of cationic surfactants, also when interacting with co-solutes and surfaces.

18. Ito TH, Miranda PCML, Morgon NH, Heerdt G, Dreiss CA, Sabadini E: **Molecular variations in aromatic cosolutes: critical role in the rheology of cationic wormlike micelles**. *Langmuir* 2014, **30**:11535–11542, https://doi.org/10.1021/la502649j.

19. Gaudino D, Pasquino R, Stellbrink J, Szekely N, Krutyeva M, Radulescu A, Pyckhout-Hintzen W, Grizzuti N: **The role of the binding salt sodium salicylate in semidilute ionic cetylpyridinium chloride micellar solutions: a rheological and scattering study**. *Phys Chem Chem Phys* 2017, **19**:782–790, https://doi.org/10.1039/C6CP06964A.

20. Lutz-Bueno V, Pasquino R, Liebi M, Kohlbrecher J, Fischer P: **Viscoelasticity enhancement of surfactant solutions depends on molecular conformation: influence of surfactant headgroup structure and its counterion**. *Langmuir* 2016, **32**: 4239–4250, https://doi.org/10.1021/acs.langmuir.6b00776.

21. Pasquino R, De Gennaro B, Gaudino D, Grizzuti N: **On the use of nonsteroidal anti-inflammatory drugs as rheology modifiers**

for surfactant solutions. *J Pharmaceut Sci* 2017, **106**: 3410–3412, https://doi.org/10.1016/j.xphs.2017.07.002.

22. * Mandal T: **Scission energy and topology of micelles controlled by the molecular structure of additives**. *Soft Matter* 2022, **18**:1678–1687, https://doi.org/10.1039/D2SM00040G.
Coarse-grained (CG) molecular dynamics simulations (MD) were used to comprehend the role of the additives molecular structure on the micellar scission energy.

23. Danino D: **Cryo-TEM of soft molecular assemblies**. *Curr Opin Colloid Interface Sci* 2012, **17**:316–329, https://doi.org/10.1016/j.cocis.2012.10.003.

24. Gaudino D, Pasquino R, Grizzuti N: **Adding salt to a surfactant solution: linear rheological response of the resulting morphologies**. *J Rheol* 2015, **59**:1363–1375, https://doi.org/10.1122/1.4931114.

25. González YI, Kaler EW: **Cryo-TEM studies of worm-like micellar solutions**. *Curr Opin Colloid Interface Sci* 2005, **10**: 256–260, https://doi.org/10.1016/j.cocis.2005.09.007.

26. Rogers SA, Calabrese MA, Wagner NJ: **Rheology of branched wormlike micelles**. *Curr Opin Colloid Interface Sci* 2014, **19**: 530–535, https://doi.org/10.1016/j.cocis.2014.10.006.

27. Zheng C, Lu H, Wang L, Huang Z: **The pH and temperature dual-responsive micelle transition in the mixture of hydrotrope potassium phthalic acid and quaternary ammonium surfactants cetyltrimethylammonium bromide**. *J Dispersion Sci Technol* 2017, **38**:1330–1335, https://doi.org/10.1080/01932691.2016.1236268.

28. Cusano I, Ionita I, Gonzalez PR, Danino D, Grizzuti N, Pasquino R: **Drug-induced transitions from micelles to vesicles in ionic surfactant solutions**. *Colloids Surf A Physicochem Eng Asp* 2024, **690**, 133793, https://doi.org/10.1016/j.colsurfa.2024.133793.

29. Lequeux F: **Reptation of connected wormlike micelles**. *EPL* 1992, **19**:675, https://doi.org/10.1209/0295-5075/19/8/003.

30. Oelschlaeger C, Schopferer M, Scheffold F, Willenbacher N: **Linear-to-Branched micelles transition: a rheometry and diffusing wave spectroscopy (DWS) study**. *Langmuir* 2009, **25**: 716–723, https://doi.org/10.1021/la802323x.

31. Zaldivar G, Conda-Sheridan M, Tagliazucchi M: **Scission energies of surfactant wormlike micelles loaded with nonpolar additives**. *J Colloid Interface Sci* 2021, **604**:757–766, https://doi.org/10.1016/j.jcis.2021.07.001.

32. Rehage H, Hoffmann H: **Rheological properties of viscoelastic surfactant systems**. *J Phys Chem* 1988, **92**:4712–4719, https://doi.org/10.1021/j100327a031.

33. Wheeler EK, Izu P, Fuller GG: **Structure and rheology of wormlike micelles**. *Rheol Acta* 1996, **35**:139–149, https://doi.org/10.1007/BF00396041.

34. Turner MS, Cates ME: **Linear viscoelasticity of wormlike micelles: a comparison of micellar reaction kinetics**. *J. Phys. II France* 1992, **2**:503–519, https://doi.org/10.1051/jp2:1992102.

35. Cates ME: **Reptation of living polymers: dynamics of entangled polymers in the presence of reversible chain-scission reactions**. *Macromolecules* 1987, **20**:2289–2296, https://doi.org/10.1021/ma00175a038.

36. Thurn H, Hoffmann H: **Evidence of sticky contacts between wormlike micelles in viscoelastic surfactant solutions**. *Langmuir* 2019, **35**:12192–12204, https://doi.org/10.1021/acs.langmuir.9b02120.

37. Cates ME, Candau SJ: **Statics and dynamics of worm-like surfactant micelles**. *J Phys Condens Matter* 1990, **2**:6869, https://doi.org/10.1088/0953-8984/2/33/001.

38. Granek R: **Dip in G''(.omega.) of polymer melts and semidilute solutions**. *Langmuir* 1994, **10**:1627–1629, https://doi.org/10.1021/la00017a051.

39. Granek R, Cates ME: **Stress relaxation in living polymers: results from a Poisson renewal model**. *J Chem Phys* 1992, **96**: 4758–4767, https://doi.org/10.1063/1.462787.

40. ** Peterson JD, Zou W, Larson RG, Cates ME: **Wormlike Micelles revisited: a comparison of models for linear rheology**. *J Non-Newtonian Fluid Mech* 2023, **322**, 105149, https://doi.org/10.1016/j.jnnfm.2023.105149.
A critical review on modeling the linear rheology of wormlike micelles and on the related ill-posed problem of extracting quantitative microscopic information.

41. Lequeux F: **Linear response of self assembling systems: mean field solution**. *J. Phys. II France* 1991, **1**:195–207, https://doi.org/10.1051/jp2:1991155.

42. Peterson JD, Cates ME: **Constitutive models for well-entangled living polymers beyond the fast-breaking limit**. *J Rheol* 2021, **65**:633–662, https://doi.org/10.1122/8.0000199.

43. Tan G, Zou W, Weaver M, Larson RG: **Determining threadlike micelle lengths from rheometry**. *J Rheol* 2020, **65**:59–71, https://doi.org/10.1122/8.0000152.

44. ** Zou W, Tan G, Weaver M, Koenig P, Larson RG: **Mesoscopic modeling of the effect of branching on the viscoelasticity of entangled wormlike micellar solutions**. *Phys Rev Res* 2023, **5**, 043024, https://doi.org/10.1103/PhysRevResearch.5.043024.
One of the many outstanding papers by Larson's group on the mesoscopic pointer algorithm applied to wormlike micelles. In this paper, the model is applied to branched micelles, it can predict branching details from linear rheology and differentiate between branches and micelles ends.

45. Zou W, Larson RG: **A mesoscopic simulation method for predicting the rheology of semi-dilute wormlike micellar solutions**. *J Rheol* 2014, **58**:681–721, https://doi.org/10.1122/1.4868875.

46. Zou W, Tan G, Jiang H, Vogtt K, Weaver M, Koenig P, Beaucage G, Larson RG: **From well-entangled to partially-entangled wormlike micelles**. *Soft Matter* 2019, **15**:642–655, https://doi.org/10.1039/C8SM02223B.

47. Tan G, Larson RG: **Quantitative modeling of threadlike micellar solution rheology**. *Rheol Acta* 2022, **61**:443–457, https://doi.org/10.1007/s00397-022-01341-4.

48. Tavera-Vázquez A, Rincón-Londoño N, López-Santiago RF, Castillo R: **Measuring mesoscopic scales in complex fluids embedded with giant cylindrical micelles with diffusing wave spectroscopy micro-rheology**. *J. Phys. Condens. Matter.* 2021, **34**, https://doi.org/10.1088/1361-648X/ac2c3e.

49. Sarmiento-Gomez E, Lopez-Diaz D, Castillo R: **Microrheology and characteristic lengths in wormlike micelles made of a zwitterionic surfactant and SDS in brine**. *J Phys Chem B* 2010, **114**:12193–12202, https://doi.org/10.1021/jp104996h.

50. Gaudino D, Costanzo S, Ianniruberto G, Grizzuti N, Pasquino R: **Linear wormlike micelles behave similarly to entangled linear polymers in fast shear flows**. *J Rheol* 2020, **64**:879–888, https://doi.org/10.1122/8.0000003.

51. Willenbacher N, Oelschlaeger C, Schopferer M, Fischer P, Cardinaux F, Scheffold F: **Broad bandwidth optical and mechanical rheometry of Wormlike Micelle Solutions**. *Phys. Rev. Lett.* 2007, **99**:068302, https://doi.org/10.1103/PhysRevLett.99.068302.

52. Rothstein JP, Mohammadigoushki H: **Complex flows of viscoelastic wormlike micelle solutions**. *J Non-Newtonian Fluid Mech* 2020, **285**, 104382, https://doi.org/10.1016/j.jnnfm.2020.104382.

53. Shi J, Rogers SA: **The benefits of a formalism built on recovery: theory, experiments, and modeling**. *J Non-Newtonian Fluid Mech* 2023, **321**, 105113, https://doi.org/10.1016/j.jnnfm.2023.105113.

54. Hyun K, Wilhelm M, Klein CO, Cho KS, Nam JG, Ahn KH, Lee SJ, Ewoldt RH, McKinley GH: **A review of nonlinear oscillatory shear tests: analysis and application of large amplitude oscillatory shear (LAOS)**. *Prog Polym Sci* 2011, **36**:1697–1753, https://doi.org/10.1016/j.progpolymsci.2011.02.002.

55. Dhont JKG, Briels WJ: **Gradient and vorticity banding**. *Rheol Acta* 2008, **47**:257–281, https://doi.org/10.1007/s00397-007-0245-0.

56. Fielding SM, Olmsted PD: **Flow phase diagrams for concentration-coupled shear banding**. *Eur Phys J E* 2003, **11**: 65–83, https://doi.org/10.1140/epje/i2002-10128-7.

57. Manneville S: **Recent experimental probes of shear banding**. *Rheol Acta* 2008, **47**:301–318, https://doi.org/10.1007/s00397-007-0246-z.

58. Porte G, Berret J-F, Harden JL: **Inhomogeneous flows of complex fluids: mechanical instability versus non-equilibrium phase transition**. *J. Phys. II France* 1997, **7**: 459–472, https://doi.org/10.1051/jp2:1997138.

59. Arenas-Gómez B, Garza C, Liu Y, Castillo R: **Alignment of worm-like micelles at intermediate and high shear rates**. *J Colloid Interface Sci* 2020, **560**:618–625, https://doi.org/10.1016/j.jcis.2019.10.052.

60. Helgeson ME, Reichert MD, Hu YT, Wagner NJ: **Relating shear banding, structure, and phase behavior in wormlike micellar solutions**. *Soft Matter* 2009, **5**:3858–3869, https://doi.org/10.1039/B900948E.

61. López-González MR, Holmes WM, Callaghan PT: **Rheo-NMR phenomena of wormlike micelles**. *Soft Matter* 2006, **2**: 855–869, https://doi.org/10.1039/B600978F.

62. Paul T Callaghan: **Rheo-NMR: nuclear magnetic resonance and the rheology of complex fluids**. *Rep Prog Phys* 1999, **62**: 599, https://doi.org/10.1088/0034-4885/62/4/003.

63. Hommel RJ, Graham MD: **Flow instabilities in circular Couette flow of wormlike micelle solutions with a reentrant flow curve**. *J Non-Newtonian Fluid Mech* 2024, **324**, 105183, https://doi.org/10.1016/j.jnnfm.2023.105183.

64. Hommel RJ, Graham MD: **Constitutive modeling of dilute wormlike micelle solutions: shear-induced structure and transient dynamics**. *J Non-Newtonian Fluid Mech* 2021, **295**, 104606, https://doi.org/10.1016/j.jnnfm.2021.104606.

65. Pasquino R, Avallone PR, Costanzo S, Inbal I, Danino D, Ianniello V, Ianniruberto G, Marrucci G, Grizzuti N: **On the startup behavior of wormlike micellar networks: the effect of different salts bound to the same surfactant molecule**. *J Rheol* 2023, **67**:353–364, https://doi.org/10.1122/8.0000537.

66. Singh PK, Lee JC-W, Patankar KA, Rogers SA: **Revisiting the basis of transient rheological material functions: insights from recoverable strain measurements**. *J Rheol* 2021, **65**: 129–144, https://doi.org/10.1122/8.0000154.

67. Liu G, Wang S-Q: **Entangled linear polymer solutions at high shear: from strain softening to hardening**. *Macromolecules* 2016, **49**:9647–9654, https://doi.org/10.1021/acs.macromol.6b02053.

68. Amin D, Wang Z: **Nonlinear rheology and dynamics of supramolecular polymer networks formed by associative telechelic chains under shear and extensional flows**. *J Rheol* 2020, **64**:581–600, https://doi.org/10.1122/1.5120897.

69. Calabrese MA, Rogers SA, Porcar L, Wagner NJ: **Understanding steady and dynamic shear banding in a model wormlike micellar solution**. *J Rheol* 2016, **60**:1001–1017, https://doi.org/10.1122/1.4961035.

70. Gaudino D, Pasquino R, Kriegs H, Szekely N, Pyckhout-Hintzen W, Lettinga MP, Grizzuti N: **Effect of the salt-induced micellar microstructure on the nonlinear shear flow behavior of ionic cetylpyridinium chloride surfactant solutions**. *Phys Rev E* 2017, **95**, 032603, https://doi.org/10.1103/PhysRevE.95.032603.

71. López-Santiago RF, Delgado J, Castillo R: **Micellar entanglement and its relation to the elastic behavior of wormlike micelle fluids**. *J Colloid Interface Sci* 2022, **626**:1015–1027, https://doi.org/10.1016/j.jcis.2022.07.003.

72. Lee JC-W, Weigandt KM, Kelley EG, Rogers SA: **Structure-property relationships via recovery rheology in viscoelastic materials**. *Phys Rev Lett* 2019, **122**, 248003, https://doi.org/10.1103/PhysRevLett.122.248003.

73. Fardin MA, Ober TJ, Grenard V, Divoux T, Manneville S, McKinley GH, Lerouge S: **Interplay between elastic instabilities and shear-banding: three categories of Taylor–Couette flows and beyond**. *Soft Matter* 2012, **8**:10072–10089, https://doi.org/10.1039/C2SM26313K.

74. Fardin MA, Perge C, Taberlet N: **"The hydrogen atom of fluid dynamics" – introduction to the Taylor–Couette flow for soft matter scientists**. *Soft Matter* 2014, **10**:3523–3535, https://doi.org/10.1039/C3SM52828F.

75. ** Datta SS, Ardekani AM, Arratia PE, Beris AN, Bischofberger I, McKinley GH, Eggers JG, López-Aguilar JE, Fielding SM, Frishman A, Graham MD, Guasto JS, Haward SJ, Shen AQ, Hormozi S, Morozov A, Poole RJ, Shankar V, Shaqfeh ESG, Stark H, Steinberg V, Subramanian G, Stone HA: **Perspectives on viscoelastic flow instabilities and elastic turbulence**. *Phys. Rev. Fluids* 2022, **7**, 080701, https://doi.org/10.1103/PhysRevFluids.7.080701.
A joint effort on resuming viscoelastic flow instabilities in every aspect, with modern questions and puzzles that motivate further studies of this fascinating subject.

76. * Rassolov P, Mohammadigoushki H: **Role of micellar entanglements on kinetics of shear banding flow formation**. *J Rheol* 2022, **67**:169–181, https://doi.org/10.1122/8.0000436.
A systematic investigation on the role of micellar entanglement number on the kinetics of shear-banding flow formation in a Taylor-Couette flow.

77. Casanellas L, Ortín J: **Vortex ring formation in oscillatory pipe flow of wormlike micellar solutions**. *J Rheol* 2014, **58**: 149–181, https://doi.org/10.1122/1.4851316.

78. Fielding SM: **Linear instability of planar shear banded flow**. *Phys Rev Lett* 2005, **95**, 134501, https://doi.org/10.1103/PhysRevLett.95.134501.

79. Wilson HJ, Fielding SM: **Linear instability of planar shear banded flow of both diffusive and non-diffusive Johnson–Segalman fluids**. *J Non-Newtonian Fluid Mech* 2006, **138**:181–196, https://doi.org/10.1016/j.jnnfm.2006.05.010.

80. Fardin MA, Ober TJ, Gay C, Grégoire G, McKinley GH, Lerouge S: **Criterion for purely elastic Taylor-Couette instability in the flows of shear-banding fluids**. *EPL* 2011, **96**, 44004, https://doi.org/10.1209/0295-5075/96/44004.

81. Perge C, Fardin M-A, Manneville S: **Inertio-elastic instability of non shear-banding wormlike micelles**. *Soft Matter* 2014, **10**: 1450–1454, https://doi.org/10.1039/C3SM52868E.

82. Rogers S, Kohlbrecher J, Lettinga MP: **The molecular origin of stress generation in worm-like micelles, using a rheo-SANS Laos approach**. *Soft Matter* 2012, **8**:7831–7839, https://doi.org/10.1039/C2SM25569C.

83. Larson RG: **A constitutive equation for polymer melts based on partially extending strand convection**. *J Rheol* 1984, **28**: 545–571, https://doi.org/10.1122/1.549761.

84. Moorcroft RL, Fielding SM: **Criteria for shear banding in time-dependent flows of complex fluids**. *Phys Rev Lett* 2013, **110**, 086001, https://doi.org/10.1103/PhysRevLett.110.086001.

85. Carter KA, Girkin JM, Fielding SM: **Shear banding in large amplitude oscillatory shear (LAOStrain and LAOStress) of polymers and wormlike micelles**. *J Rheol* 2016, **60**:883–904, https://doi.org/10.1122/1.4960512.

86. Rogers SA, Lettinga MP: **A sequence of physical processes determined and quantified in large-amplitude oscillatory shear (LAOS): application to theoretical nonlinear models**. *J Rheol* 2012, **56**:1–25, https://doi.org/10.1122/1.3662962.

87. ** Shim YH, Singh PK, Rogers SA: **Unified interpretation of MAOS responses via experimentally decomposed material functions**. *J Rheol* 2023, **67**:1141–1158, https://doi.org/10.1122/8.0000702.
A new analysis on MAOS material functions for wormlike micelles that can unify the interpretation of the Chebyshev and sequence of physical processes analyses via experimentally decomposed material functions.

88. Ewoldt RH, Hosoi AE, McKinley GH: **New measures for characterizing nonlinear viscoelasticity in large amplitude oscillatory shear**. *J Rheol* 2008, **52**:1427–1458, https://doi.org/10.1122/1.2970095.

89. Chellamuthu M, Rothstein JP: **Distinguishing between linear and branched wormlike micelle solutions using extensional rheology measurements**. *J Rheol* 2008, **52**:865–884, https://doi.org/10.1122/1.2896120.

90. Yesilata B, Clasen C, McKinley GH: **Nonlinear shear and extensional flow dynamics of wormlike surfactant solutions**. *J Non-Newtonian Fluid Mech* 2006, **133**:73–90, https://doi.org/10.1016/j.jnnfm.2005.10.009.

91. Fischer P, Fuller GG, Lin Z: **Branched viscoelastic surfactant solutions and their response to elongational flow**. *Rheol Acta* 1997, **36**:632–638, https://doi.org/10.1007/BF00367359.

92. Prud'homme RK, Warr GG: **Elongational flow of solutions of rodlike micelles**. *Langmuir* 1994, **10**:3419–3426, https://doi.org/10.1021/la00022a010.

93. Walker LM, Moldenaers P, Berret J-F: **Macroscopic response of wormlike micelles to elongational flow**. *Langmuir* 1996, **12**:6309–6314, https://doi.org/10.1021/la960662v.

94. Du J, Ohtani H, Owens CE, Zhang L, Ellwood K, McKinley GH: **An improved Capillary Breakup Extensional Rheometer to characterize weakly rate-thickening fluids: applications in synthetic automotive oils**. *J Non-Newtonian Fluid Mech* 2021, **291**, 104496, https://doi.org/10.1016/j.jnnfm.2021.104496.

95. Bhardwaj A, Miller E, Rothstein JP: **Filament stretching and capillary breakup extensional rheometry measurements of viscoelastic wormlike micelle solutions**. *J Rheol* 2007, **51**:693–719, https://doi.org/10.1122/1.2718974.

96. Sur S, Rothstein J: **Drop breakup dynamics of dilute polymer solutions: effect of molecular weight, concentration, and viscosity**. *J Rheol* 2018, **62**:1245–1259, https://doi.org/10.1122/1.5038000.

97. Dinic J, Zhang Y, Jimenez LN, Sharma V: **Extensional relaxation times of dilute, aqueous polymer solutions**. *ACS Macro Lett* 2015, **4**:804–808, https://doi.org/10.1021/acsmacrolett.5b00393.

98. * Zinelis K, Abadie T, McKinley GH, Matar OK: **The fluid dynamics of a viscoelastic fluid dripping onto a substrate**. *Soft Matter* 2024, **20**:8198–8214, https://doi.org/10.1039/D4SM00406J.
A numerical approach using the open-source code Basilisk has been used to successfully capture the two main fluidodynamic regimes that drive the filament thinning in dripping-onto-substrate (DoS) rheometry.

99. Omidvar R, Wu S, Mohammadigoushki H: **Detecting wormlike micellar microstructure using extensional rheology**. *J Rheol* 2019, **63**:33–44, https://doi.org/10.1122/1.5050387.

100. Rothstein JP: *Strong flows of viscoelastic wormlike micelle solutions.* 2009.

101. Chen C-M, Warr GG: **Light scattering from wormlike micelles in an elongational field**. *Langmuir* 1997, **13**:1374–1376, https://doi.org/10.1021/la960950r.

102. Dubash N, Cheung P, Shen AQ: **Elastic instabilities in a microfluidic cross-slot flow of wormlike micellar solutions**. *Soft Matter* 2012, **8**:5847–5856, https://doi.org/10.1039/C2SM25215E.

103. Pathak JA, Hudson SD: **Rheo-optics of equilibrium polymer solutions: wormlike micelles in elongational flow in a microfluidic cross-slot**. *Macromolecules* 2006, **39**:8782–8792, https://doi.org/10.1021/ma061355r.

104. Zhao Y, Q Shen A, J Haward S: **Flow of wormlike micellar solutions around confined microfluidic cylinders**. *Soft Matter* 2016, **12**:8666–8681, https://doi.org/10.1039/C6SM01597B.

105. Stone PA, Hudson SD, Dalhaimer P, Discher DE, Amis EJ, Migler KB: **Dynamics of wormlike micelles in elongational flows**. *Macromolecules* 2006, **39**:7144–7148, https://doi.org/10.1021/ma0611016.

106. Salipante PF, Little CAE, Hudson SD: **Jetting of a shear banding fluid in rectangular ducts**. *Phys. Rev. Fluids* 2017, **2**, 033302, https://doi.org/10.1103/PhysRevFluids.2.033302.

107. Singh P, Sharma K, Puchades I, Agarwal PB: **A comprehensive review on MEMS-based viscometers**. *Sensor Actuator Phys* 2022, **338**, https://doi.org/10.1016/j.sna.2022.113456.

108. Haward SJ, Shen AQ: **Microfluidic flows and confinement of wormlike micelles**. *RSC Soft Matter* 2017:236–278, https://doi.org/10.1039/9781782629788-00236. 2017-January.

109. Zhao Y, Cheung P, Shen AQ: **Microfluidic flows of wormlike micellar solutions**. *Adv Colloid Interface Sci* 2014, **211**:34–46, https://doi.org/10.1016/j.cis.2014.05.005.

110. ** Varchanis S, Haward SJ, Hopkins CC, Tsamopoulos J, Shen AQ: **Evaluation of constitutive models for shear-banding wormlike micellar solutions in simple and complex flows**. *J Non-Newtonian Fluid Mech* 2022, **307**, 104855, https://doi.org/10.1016/j.jnnfm.2022.104855.
Constitutive models for shear-banding wormlike micellar solutions were critically compared with specific care to their inability to quantitatively describe the nonlinear regime, in particular in extensional flows and with elastic instabilities.

111. Pasquino R, Droghetti H, Carbone P, Mirzaagha S, Grizzuti N, Marchisio D: **An experimental rheological phase diagram of a tri-block co-polymer in water validated against dissipative particle dynamics simulations**. *Soft Matter* 2019, **15**:1396–1404, https://doi.org/10.1039/C8SM01959B.

112. Fetsch C, Gaitzsch J, Messager L, *et al.*: **Self-assembly of amphiphilic block copolypeptoids – Micelles, worms and polymersomes**. *Sci. Rep.* 2016, **33491**, https://doi.org/10.1038/srep33491.

113. Tavera-Vázquez A, Arenas-Gómez B, Garza C, Castillo R: **Structure, rheology, and microrheology of wormlike micelles made of PB–PEO diblock copolymers**. *Soft Matter* 2018, **14**:7264–7276, https://doi.org/10.1039/C8SM01530A.